Korean J. Chem. Eng., 39(1), 189-197 (2022)
DOI: 10.1007/s11814-021-0900-7

pISSN: 0256-1115
eISSN: 1975-7220

Experimental investigation of polysulfone modified cellulose acetate membrane for CO_2/H_2 gas separation

Inamullah Douna*, Sarah Farrukh*,†, Arshad Hussain, Zarrar Salahuddin*, Tayyaba Noor*, Erum Pervaiz*, Mohammad Younas***, and Xian Feng Fan****

*School of Chemical and Material Engineering, National University of Science and Technology, Islamabad, Pakistan
**Pak-Austria Fachhochschule, Institute of Applied Science and Technology, Haripur-KPK, Pakistan
***Department of Chemical Engineering, University of Engineering and Technology, Peshawar, Pakistan
****Department of Chemical Engineering, University of Edinburgh, Edinburgh, UK
(*Received 11 March 2021 • Revised 21 June 2021 • Accepted 12 July 2021*)

Abstract−Processed gas streams from the water gas shift reactor (WGSR) are enriched with CO_2 and H_2. Purification of H_2 from CO_2 for different applications is required because of its environmental and economic benefits. Among different separation technologies, membrane technology gets much attention due to its various advantages. In this work, cellulose acetate/polysulfone blended membranes were fabricated via solution casting method for CO_2/H_2 separation. The separation performance of pure CA membrane was enhanced by addition of PSF. The fabricated membranes were analyzed through various characterization techniques, such as FTIR, SEM, DSC, and XRD. Gas permeation results show that permeability of CO_2 increased with increasing concentration of PSF. Notable permeability (P=80.51 Barrer) of CO_2 and selectivity of CO_2/H_2=1.83 of CA/PSF 2 wt% were achieved at 25 °C and 2.5 bar compared to pure CA membrane. To the best of our knowledge, this blend has been studied for the first time for gas separation, prepared through the solution casting method.

Keywords: Cellulose Acetate, Polysulfone, Water-gas Shift Reaction, Polymer Blend, CO_2/H_2 Separation Membrane

INTRODUCTION

There is an unprecedented demand for renewable energy worldwide [1]. Hydrogen is a promising solution since it is a highly efficient, sustainable, and clean energy fuel that generates only water as products upon combustion [2-4]. On an industrial scale, two processes, coal gasification and steam reforming of natural gas, are predominantly being used to produce hydrogen. These processes are followed by water gas shift reaction to reduce the concentration of CO; meanwhile, H_2 and electricity are generated. The gas stream from WGSR mainly contains a mixture of CO_2 and H_2; thus it is necessary to purify downstream gas to obtain high purity H_2 for industrial-scale applications [4,5]. The chemical equation for WGSR is as follows:

$$H_2+CO+H_2O \rightarrow CO_2+2H_2$$

Conventional separation technologies, such as amine wet scrubbing and pressure swing adsorption, have been utilized for the separation of CO_2 from H_2 [6-9]. Since two decades, the membrane is recognized as an attractive separation technique due to its simplicity in operation and high energy efficiency with small carbon footprint. All of these advantages make it a more suitable choice for gas separation as compared to other technologies [10-12]. Two types of membrane are being used for the separation of CO_2 from H_2: CO_2-selective membrane and H_2-selective membrane. Although H_2-selective membranes are more common due to easy permeation of H_2 based on its small kinetic diameter [13-15], there are examples of CO_2-selective membrane as well. These CO_2-selective membranes offer many advantages over H_2-selective membranes from an industrial point of view. as the reduction in H_2 compression cost subsequently makes it cost-effective in transportation and storage [16,17].

Research is being conducted on polymers for the fabrication of membranes other than ceramics or metals due to ease of processability. Numbers of polymers like cellulose acetate (CA) [18,19], polyvinyl alcohol (PVA) [20], cellulose triacetate (CTA) [21], polyurethane (PU) [22], polysulfone (PSF) [23], polyethylene oxide (PEO) [24], polyimides (PI) [25] and polyphenylene oxide (PPO) [26] have been explored for gas separation. The practical applicability of pure polymeric membrane is limited due to the tradeoff between permeability and selectivity. To overcome this limitation, different strategies have been reported, such as cross-linking [27], polymer blending [28,29], and mixed matrix membranes (MMMs) [30]. Among various attractive modification strategies, polymer blending is promising due to its simplicity and ease of fabrication. A unique property of two or more polymers can be attained if the polymers are compatible with each other [31].

Various successful combinations of polymers blends are reported in the literature. In previous years, many researchers worked on blended membranes for CO_2/H_2 separation [32,33]. Rabiee et al. investigated the effect of glycerol triacetate (GTA) in Pebax 1657 membrane to improve CO_2/H_2 separation performance [34]. They

†To whom correspondence should be addressed.
E-mail: sarah.farrukh@scme.nust.edu.pk

showed an increment in both sorption and diffusion coefficients of gases by incorporation of GTA. The results revealed the increment of CO_2/H_2 selectivity by 100% almost doubled after incorporation of GTA in Pebax 1657 membrane. Reijerkerk et al. prepared Pebax 1657 membrane blended with varying composition of additive (PDMS 20 wt%-PEG 80 wt%) [35]. These blends showed maximum CO_2 permeability of 98 barrers with remarkable selectivity CO_2/H_2 of 9.5 at 50 wt% PDMS-PEG loading. Sanaeepur et al. reported that blending of PEBAX 1657 with CA increased the separation performance of the membrane [36]. They concluded that the solubility of CO_2 improved and hence the permeability of CO_2 increased with the incorporation of PEBAX 1657. Hamid investigated the blending features of polysulfone-polyimide (PSF/PI) blended flat sheet membrane at different solvent evaporation times to study the separation performance of H_2/CO_2 [37]. The results revealed that the selectivity of H_2/CO_2 was high, which is 4.4 as compared to pure PSF (2.9) and PI (3.1) membranes. Additionally, a few investigators utilized blends of different polymers CA/PEG [38,39], CA/CL [40], and s-PEEK/Matrimid [41] for improving the membrane separation performance in CO_2 separating processes. The gas separation performance of polymer blended membranes depends on two factors: compatibility of the blending polymers and their microstructure arrangement of blends.

Among the well known commercialized polymers, CA possesses excellent mechanical and thermal properties, superior film-making ability, and renewable resources of raw material [42,43]. However, the only drawback is its low selectivity for CO_2/H_2 [33,44]. To enhance the selectivity of CO_2/H_2, polysulfone (PSF) was selected to blend with CA without compromising the permeability. PSF has phenyl rings and stable functional sulfonate groups. These groups have a strong affinity with polar CO_2, which leads to an increase in permeability of CO_2. Numerous polymeric blended membranes, including PSF in combination with other polymers, have also been reported. Thus, all these findings are encouraging that PSF can affect the permeation properties of the membrane [45-47].

Keeping in mind all the facts discussed earlier, it was planned to fabricate a CA-based PSF blended membrane with different compositions for the separation of CO_2/H_2 gas pair. Various characterization techniques, FTIR, DSC, SEM and XRD, were employed to confirm the compatibility and structural changes of subsequent CA-PSF membranes. Previously, this type of blend CA-PSF was used for water purification. According to our knowledge, this kind of blend is first time being used for gas separation.

EXPERIMENTAL WORK

1. Materials

Polysulfone (M_w 2,200), cellulose acetate (M_w 50,000, n20/D1.475) polymer were procured from Sigma Aldrich. The solvent used for membrane preparation was tetrahydrofuran (THF), which was also procured from Yuri Shanghai Chemical. Lab scale high purity CO_2 and H_2 gases were supplied by Paradise company, Pakistan.

2. Synthesis of Membrane

Polysulfone beads were kept in an oven at 60 °C to remove moisture. 1 gm of cellulose acetate was mixed with different weights of Polysulfone (20, 60,100, and 150 mg) in 10 ml of THF with overnight stirring. Next, the trapped air bubbles were detached from the solution through the degassing process. After that solution was cast on a glass slide with a doctor blade and dried in the open air. After 24 hrs the dried membranes were easily removed from the glass slide. For complete removal of the solvent, all samples were placed in oven for 6 hr and 50°.

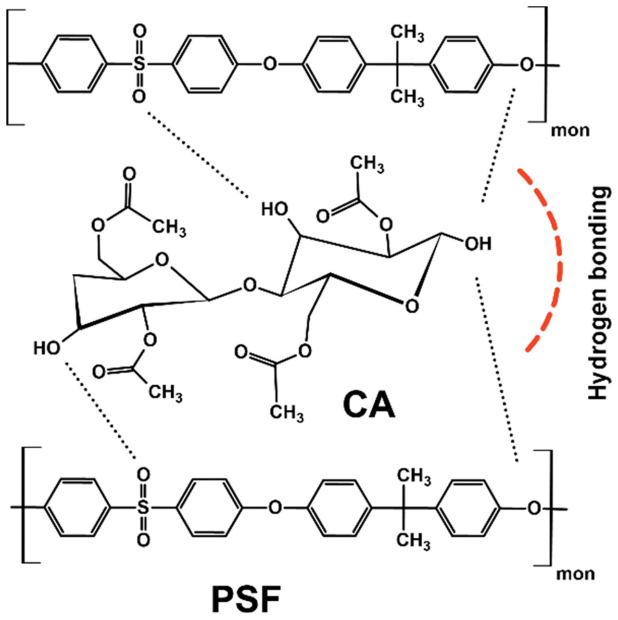

Fig. 1. Structure representation of cellulose acetate (CA) and polysulfone (PSF).

3. Gas Permeability Testing

The permeation of CO_2 and H_2 was measured at gauge pressure of 2.5 bar. The 1atm pressure was kept constant at permeate end, while the pressure on feed side was set as needed. The flow diagram of permeation (PHILOS type) setup has been shown in Fig. 2. Each membrane sample was prepared according to the size of two porous support disks. To record the volumetric flow rate of permeate, a bubble flow meter was connected with the permeate line. Each composition of the membrane was tested thrice for confirmation of results. The following equations were used for measuring gas transportation properties Eq. (1)-(2).

$$\frac{P_i}{\Delta l} = \frac{Q_i}{A\Delta p} \tag{1}$$

P_i is defined as the permeability of gases measured in Barrer as (1 Barrer=10^{-10} cm^3 (STP) cm/cm^2 s cm Hg). A is an active membrane area (cm^2). Q_i is the volumetric flowrate (cm^3(STP)/s) of permeate gas flowing through the active membrane area of (8 cm^2). Δl is the total membrane thickness in cm. And Δp (cmHg) represents the pressure difference across the membrane. The ideal selectivity can be calculated by using a simple formula, Eq. (2).

$$\alpha\left(\frac{CO_2}{H_2}\right) = \frac{P_{CO_2}}{P_{H_2}} \tag{2}$$

4. Membrane Characterization

Surface and cross-sectional morphology of pure cellulose acetate membrane along with different weight percentages of PSF blended

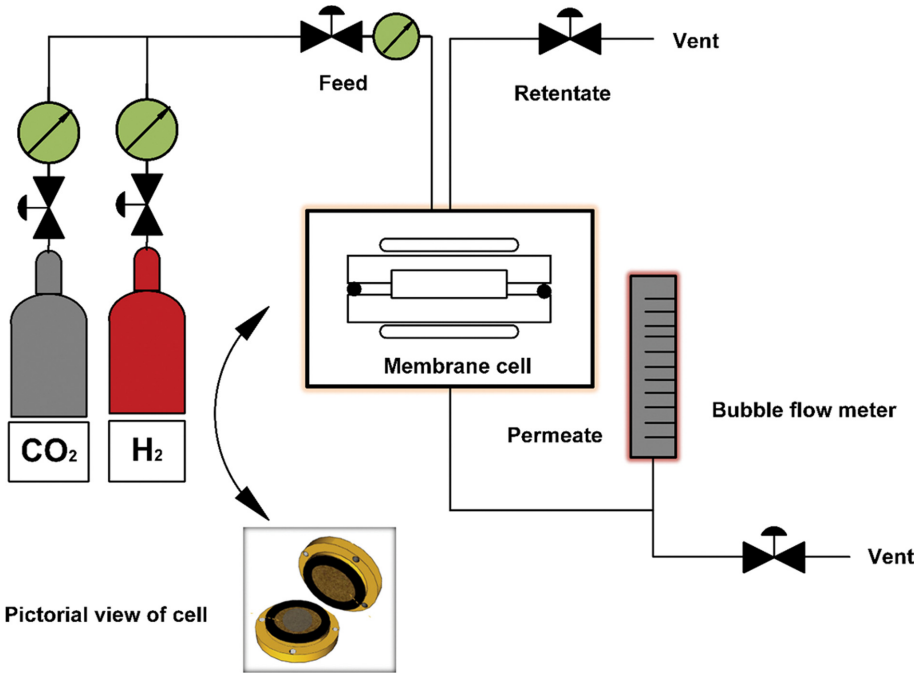

Fig. 2. Flow diagram of permeation experiment setup.

membranes were examined using JEOL, JSM-6490LA (Scanning electron microscopy). Membranes were coated with thin film of gold and then images were taken at a magnification of 3,000× and 10,000× at voltage of 10 kv.

Thermal analysis of pristine CA and all blend membranes was carried using a DSC250TA differential scanning calorimeter (DSC). The range of temperature, 25-250 °C, was set with the heating rate of 10 °C/min. Flow rate of nitrogen (10 ml/min) was maintained to remove produced gases during the DSC analysis. FTIR analysis of pure and blended membranes was done for the qualitative analysis. Perkin Elmer Spectrum 100 FTIR spectrometer was used to record FTIR spectrum at wavenumber of 4,000-400 cm^{-1}. Structural properties of synthesized membranes were analyzed on equipment from STOE, Germany. XRD pattern of all samples were taken at Scan angle 5-60° with step size of 0.01°. The radiation used for XRD analysis was Cu K α^{-1}.

RESULTS AND DISUSSION

1. FTIR Analysis of Membrane

FTIR spectroscopy is an important characterization technique used to study the physical and chemical interaction between different materials. The peaks appearing in the FTIR spectrum demonstrate the presence of different functional groups in polymeric membranes. Fig. 3 illustrates the FTIR spectra of pure CA, PSF, CA/PSF 2 wt%, CA/PSF 4 wt%, CA/PSF 6 wt%, and CA/PSF 8 wt% blend membranes. For pure CA membrane, the O-H absorption band was detected around 3,629-3,369 cm^{-1}. Furthermore, the peaks observed at wavenumbers 1,251, 2,942, 1,373 and 1,746 cm^{-1} confirmed the presence of C-O (stretching), CH_3 (asymmetric stretching), CH_3 (symmetric deformation) and C=O (stretching), respectively [36,48,49]. It is also observed from FTIR spectra of pure PSF

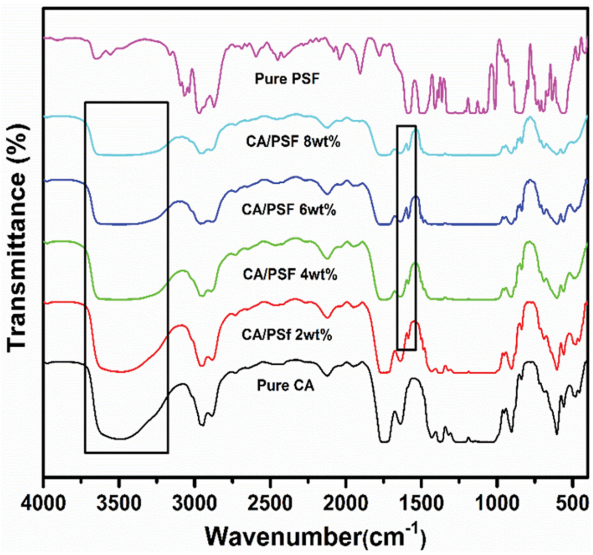

Fig. 3. FT-IR spectra of pure CA, Pure PSF, CA/PSF 2 wt%, CA/PSF 4 wt%, CA/PSF 6 wt% and CA/PSF 8 wt% blends membrane.

membrane that the stretching frequencies at 1,367 cm^{-1} and 1,162 cm^{-1} were associated with the asymmetric and symmetric vibration of sulfonate group (S=O). While the benzene ring stretching was observed at 1,487 cm^{-1}. C=C bond stretch of aromatic ring was also observed at a wavenumber of 1,590 cm^{-1}. In addition, the C-H bond of aliphatic and aromatic rings was detected at 2,985 cm^{-1} and 3,160 cm^{-1}, respectively. These characteristics peaks of the PSF membrane were also verified from the literature [37,50].

To check the presence and miscibility of PSF with the CA matrix, FTIR analysis of the blend membrane was also performed. One additional peak of C=C bond of benzene in FTIR spectra of CA/

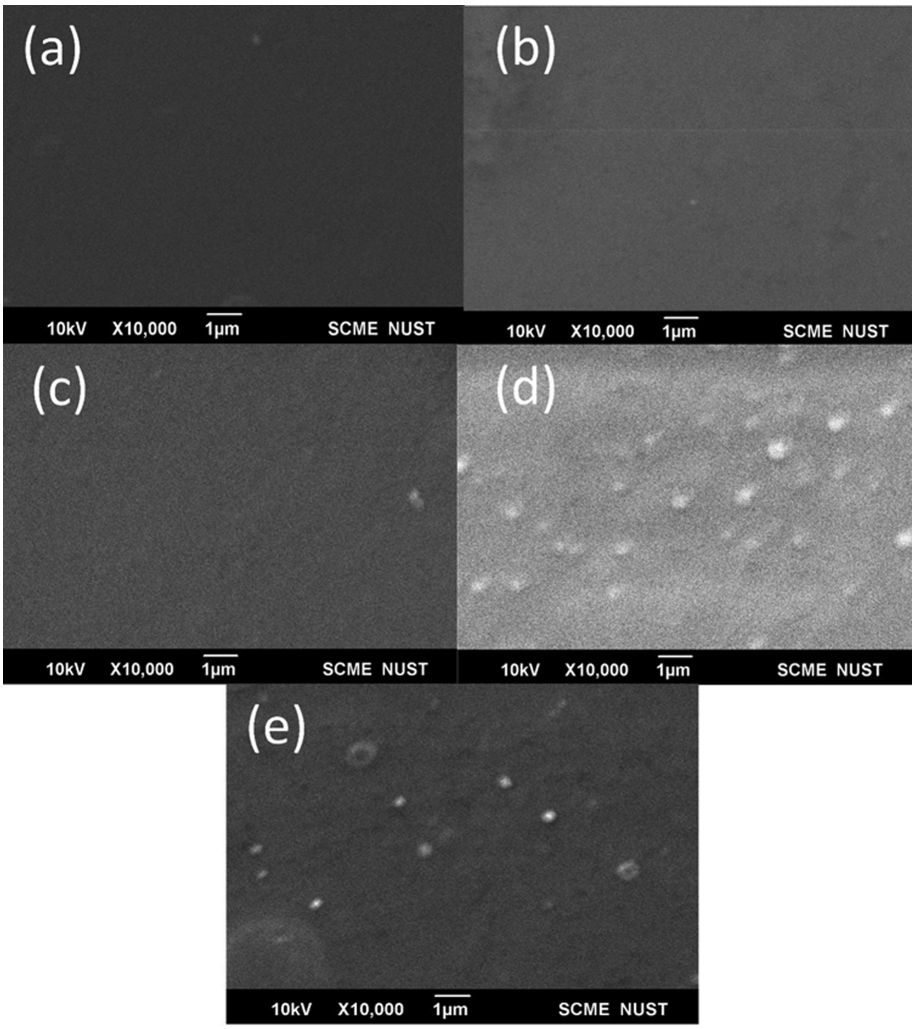

Fig. 4. SEM surface micrograms of all membranes (a) Pure CA, (b) CA/PSF 2 wt%, (c) CA/PSF 4 wt%, (d) CA/PSF 6 wt%, (e) CA/PSF 8 wt%.

PSF 2 wt%, 4 wt%, 6 wt%, and 8 wt% was detected around 1,581-1,594 cm^{-1}, which depicted the interaction of PSF with CA. The clear peak at the wave number of 3,657-3,213 cm^{-1} is ascribed the OH group, which is broadened with the increment of PSF content. Further, as such, no new peaks were observed in FTIR spectrum of all CA/PSF membranes, which confirmed that the interaction of CA with PSF is of physical nature.

2. SEM Analysis of Membrane

Surface and cross-view SEM images of pure CA and blended membrane, i.e., PSF 2 wt%, 4 wt%, 6 wt%, and 8 wt% are shown in Fig. 4 and Fig. 5. SEM micrographs of all membranes were captured at 10,000× and 3,000× magnification. From SEM images of CA, a dense and homogeneous structure without any defect is formed. The top view of CA/PSF 2 wt% and CA/PSF 4 wt% blended membrane clearly showed dense and smooth morphology without any cracks. However, some particles can be seen on the surface of CA/PSF 6 wt% and 8 wt% blended membranes. Ellipsoidal type of PSF particles were observed in cross-view images of all blended membranes except CA/PSF 2 wt% membrane, which shows good compatibility with CA matrix at this composition. The domain size of these particles was augmented as the weight percent of PSF increased from 4 to 8 wt%. The SEM images also revealed the presence of cavities in the cross-section of CA/PSF 4, 6, and 8 wt% membrane due to extraction of nodules, that is, the consequence of strong interfacial tension and coalescence [47,48,51,52].

FTIR analysis revealed that PSF interacted via hydrogen bonding with hydroxyl groups on CA; also, the schematic representation is shown in Fig. 1. Initially at PSF 2 wt%, the interaction is predominantly hydrogen bonding between sulfonate and hydroxyl groups. With increasing the quantity of PSF, the chain length increases. However, the interactive functional groups decrease [53]. It can be assumed that agglomerates formed at interface of two polymers are due to the π-π interactions or hydrophobic interaction between the PSF particles, especially at higher concentration. This may result in localizing the PSF molecule at the interface of the two-polymer phase. That gives rise to the ellipsoidal domain in the SEM images [54]. Moreover, all membranes showed a dense structure, which is favorable for gas separation. Hence it was decided that only PSF 2 wt% composition is optimum and has good compatibility for the successive formation of uniform membrane.

3. Thermal Analysis of Membranes

DSC analysis evaluated the glass transition temperature, melt-

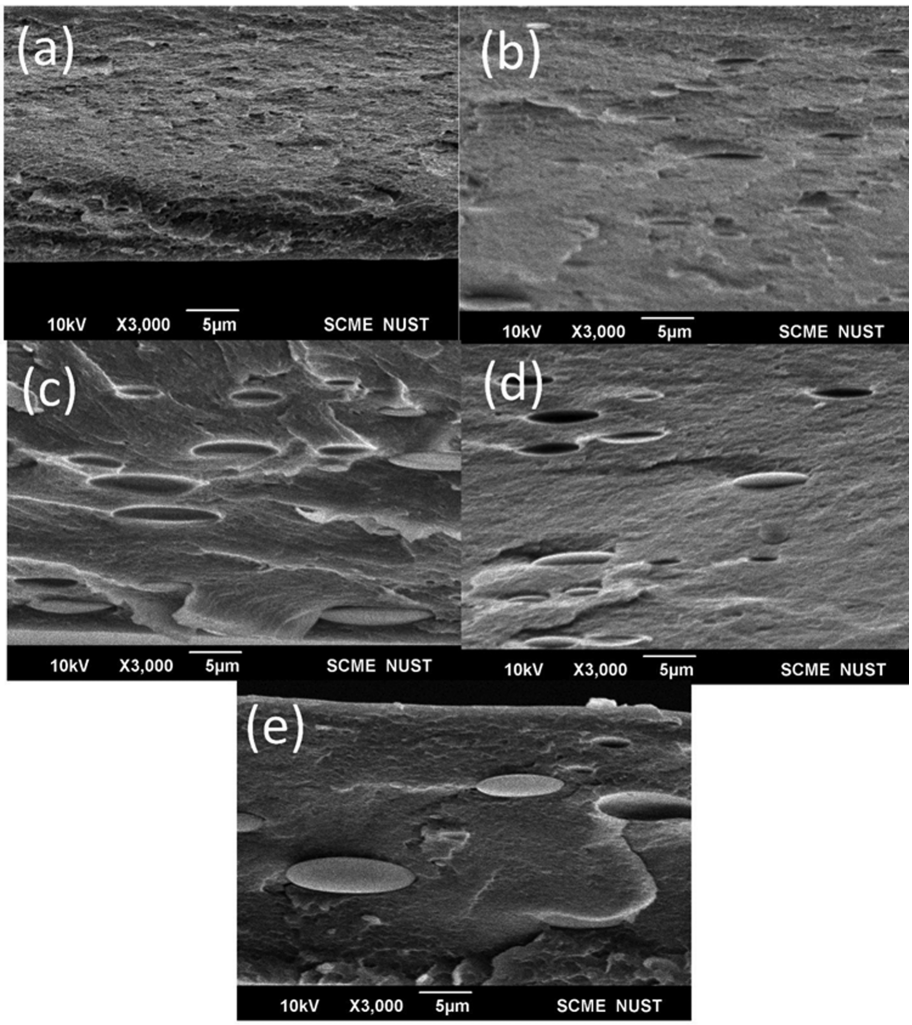

Fig. 5. SEM surface micrograms of all membranes (a) Pure CA, (b) CA/PSF 2 wt%, (c) CA/PSF 4 wt%, (d) CA/PSF 6 wt%, (e) CA/PSF 8 wt%.

ing point, and crystallinity of polymeric blended membranes. The glass transition temperature is mostly used to estimate the miscibility of polymer blends. The single glass transition temperature appearing on the DSC thermo-gram showed that the polymeric blend was miscible [55]. DSC curves of pristine CA and sequence of CA/PSF blended membrane represented in Fig. 6. Pure CA displayed glass transition temperature at about 193 °C, which is analogous to previous findings published by Sanaeepur et al. [36]. The addition of PSF increased the Tg of the blended membrane, which resulted in increment of hardness of polymer membranes. The CA/PSF 2 wt% membrane showed glass transition of 195 °C, which is higher than pure CA membrane. This increment in Tg value, particularly at CA/PSF 2 wt%, composition is due to strong interfacial interaction via hydrogen bonding between hydroxyl and sulfonate groups, therefore restricting the flexibility of CA chains [56]. Referring to glass transition temperature at 4, 6 wt% of PSF blended membrane was comparatively more than CA/PSF 2 wt% membrane. This can be due to the low affinity between PSF and CA, particularly at higher concentration leading to formation of ellipsoidal agglomerates. These agglomerates contracted the polymeric chains during membrane fabrication. This could result in restriction in the rotation of CA segments around the main chain bonds and, consequently, in higher Tg values in the prepared membranes.

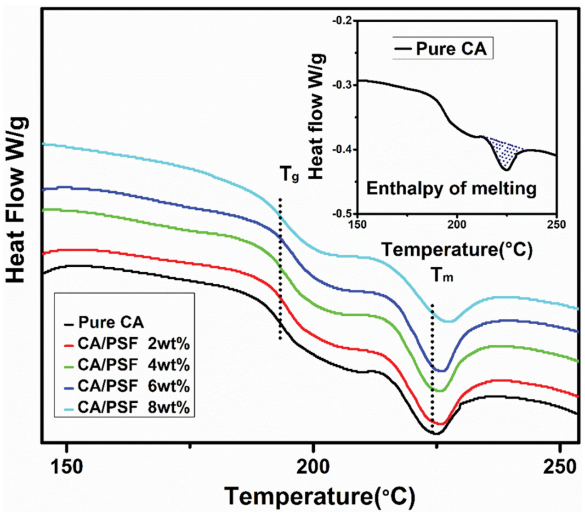

Fig. 6. DSC curves of pristine CA and blend membrane.

Table 1. DSC findings of pure CA and all blend membranes

Membrane samples	T_g (°C)	T_m (°C)	Crystallinity (%)
CA	190.27	223.73	24.7
CA/PSF 2 wt%	195.04	225.28	32
CA/PSF 4 wt%	197.16	226.20	30
CA/PSF 6 wt%	198.16	227.55	29
CA/PSF 8 wt%	194.60	228.67	25

However, at 8 wt% of PSF blended membrane, decrement in TG was observed, which resulted due to high agglomeration. This caused separation of both polymer phases, increment in free volume and reduced interaction [57]. Table 1 summarizes the data extracted from DSC findings. The crystallinity of pristine and CA/PSF blended membranes was also determined by using the following formulas:

$$X_C = \frac{\Delta H_m}{\Delta H^o} \times 100 \quad \Delta H_m = \frac{\text{The area under the melting peaks}}{\text{Heating rate}}$$

where ΔH_m is the enthalpy of melting, calculated by integration of the area under melt peaks using Origin Pro software. ΔH^o is the enthalpy of pure CA when it is 100% crystalline, that is 58.8 (J/g) [58]. As mentioned in Table 1, the shift in T_g and T_m with the amount of PSF is not as significant, which may be because PSF amount was lower than 20 wt% [59]. Furthermore, a change in crystallinity of the CA/PSF membrane was observed after the incorporation of PSF 2 wt%. Results of DSC showed decrement in crystallinity at a higher concentration of PSF, which indicates the poor miscibility behavior of the blend. As the concentration increased and reached 8 wt%, the value of crystallinity suddenly decreased. This decrement in crystallinity of blended membranes may be due to the disruption of the interchain hydrogen bonding, which results in formation of steps and kinks with more irregular structure having more free volume in prepared membrane [60,61]. This is further consolidated by SEM micrograms.

4. XRD Analysis

Structural analysis of pure and blended polymeric membranes is well investigated using the XRD technique. In general, polymer microstructure consists of crystalline and amorphous regions. In the XRD spectrum, peaks with high and sharp intensity reveal the crystalline part, while peaks with broad and lower intensity confirm the presence of the amorphous part of the polymer [40]. Fig. 7 illustrates XRD patterns of pure CA, PSF, and blended membranes. The XRD spectrum of pristine CA presents three sharp crystalline peaks at 2θ=22°, 26°, and 29° along with two broad diffuse amorphous peaks located at a diffraction angle of 2θ=10° and 17°. CA is a semi-crystalline polymer. Its low crystallinity is due to strong intermolecular interaction (hydrogen bonding) between acetyl and hydroxyl groups. The pristine PSF displayed a single spread diffraction peak at 2θ=18° due to its semi-crystalline nature (42% crystallinity) [62]. All signature peaks of pristine CA and PSF strongly agree with previous literature [59,63-66].

The XRD pattern of CA-PSF blended membrane is shown in Fig. 7. It was noticed that in the XRD spectrum of CA-PSF membrane no peak of PSF was observed, suggesting that the amorphous phase of CA is dominant [67]. Also found was that adding

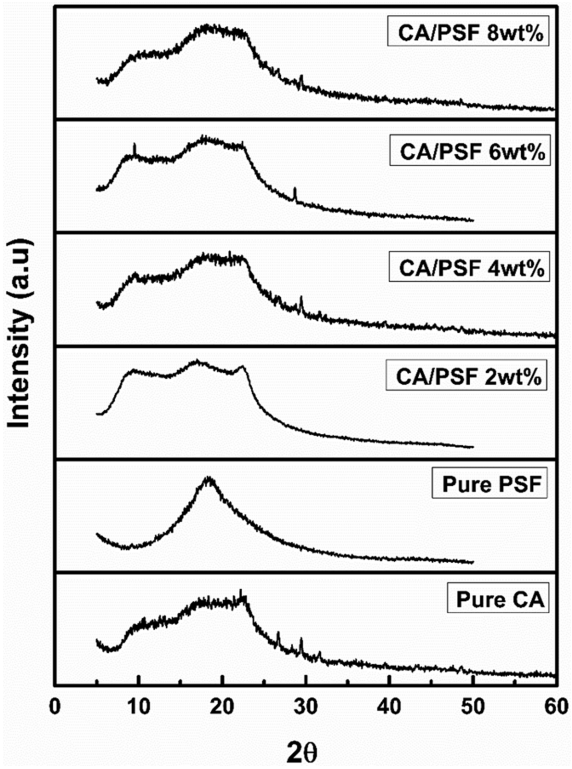

Fig. 7. XRD patterns of Pure CA, PSF and CA/PSF 2, 4, 6 and 8 wt% membranes.

the PSF with different weight percentages increased the peak intensity of the blended membrane. Maximum peak intensity was observed for PSF 2 wt% and PSF 6 wt% membranes. The increase in peak intensity shows the improvement in the crystallinity of hybrid membranes. An increase in crystallinity is also verified from DSC findings. The main reason behind the increment of crystallinity is due to interfacial interaction between two polymers [68].

5. Gas Permeation Analysis

CO_2 and H_2 gas permeation experiment were carried out to investigate the transport properties of pristine CA and blended membranes at 2.5 bar and room temperature. Gas permeation via dense membrane is governed by the solution diffusion model. The permeability of gas is based on the diffusivity and solubility of particular gas in a membrane. Solubility is related to the affinity of gas molecules with the polymer functional groups, whereas diffusivity is linked with the amount of free volume between polymer chains and kinetic diameter of gas [69,70]. The permeation results in terms of permeability and perm selectivity of CO_2 and H_2 are shown in Table 2. The recorded permeation data showed that an increase in the contents of PSF had a positive effect on the permeability of both gases. Pure CA membrane shows permeability values of 34.54 and 47.54 Barrer for CO_2 and H_2, respectively. The maximum permeability of 90.88 Barrer for CO_2 was attained at 8 wt% of PSF. Hydrogen has the highest diffusion coefficient as compared to CO_2 due to its small kinetic diameter, so it permeates preferentially through the membrane [71]. Conversely, despite having a small size, the permeability of H_2 decreased from 47.54 to 43.90 Barrer at PSF 2 wt%. This is because incorporation of PSF in CA increased crystallinity

Table 2. Single gas performance of pure CA and with different loading of PSF at room temperature and 2.5 bar

Membrane samples	Permeability (Barrer)		Selectivity (CO_2/H_2)
	CO_2	H_2	
Pure CA	34.54	47.54	0.73
CA/PSF 2 wt%	80.51	43.90	1.833861
CA/PSF 4 wt%	84.48	55.48	1.522711
CA/PSF 6 wt%	87.88	61.88	1.420168
CA/PSF 8 wt%	90.88	70.67	1.285977

Table 3. Critical temperature and kinetic diameter of feed gases

Gas	Critical temperature (T_C) [K]	Kinetic diameters (Å)
H_2	33.3	2.89
CO_2	304.2	3.30

of CA/PSF membranes, supported by XRD and DSC results. In general, the increase in crystallinity reduces the free volume in polymer membrane, which results in decrement of H_2 permeability at 2 wt% PSF blended membrane [47].

Based on these outcomes, the ideal selectivity of CO_2/H_2 was also assessed. It was found that highest CO_2/H_2 selectivity of 1.833 was observed at PSF 2 wt% blended membrane compared to pure CA membrane, which is 0.7. At a higher concentration of PSF, the selectivity of the blended membrane was reduced. This decrease in selectivity is because of the higher concentrations of PSF, which leads to the formation of cavities and micro voids at the interface of two-phase as shown in SEM micrograph. Overall, it can be stated that the CA/PSF 2 wt% was an optimized composition that gives the good permeation results. In general, permeation findings of the CA/PSF blended membrane were very significant and fascinating. The CO_2 displays higher permeability than H_2 because of the following reasons: (1) ease of condensability than H_2 due to its high critical temperature, shown in Table 3, (2) Strong affinity of CO_2 with polar groups of PSF [72]. Moreover, in CO_2, carbon is centered with two positive charge carbonyl groups. This Lewis acid base interaction developed between carbonyl groups of CO_2 and electron withdrawing oxygen in sulfonate group of PSF makes a condition for ease in transportation of CO_2 through blended membrane [73]. Consequently, solubility and thus permeability of CO_2 increased as compared to H_2 with increasing wt% of PSF [74-75].

6. Evaluation with other Studies

Table 4 summarizes the results obtained from different studies using blended membranes for CO_2 and H_2 separation operated under various conditions to furnish evaluation with our results and its general standing. Prepared membranes showed better selectivity than any other reported blend. Also, membranes with higher permeability and selectivity were operated under high temperature and pressure conditions. Whereas our blended membranes performed at lower pressure and room temperature to avoid the requirement of extra energy. Furthermore, the results show that there is considerable room for improvement in separation performance. This can be done using compatibilizers to increase the interfacial adhesion between the two polymers.

CONCLUSIONS

CA/PSF blended membranes with different concentration of PSF have been successfully prepared and investigated for CO_2/H_2 separation. In the present work, a detailed comparison of FTIR spectra of pristine CA and all CA/PSF blended membranes shows that there is only physical interaction between the polymers. DSC analysis shows a slight increase in T_m of all blended membranes, which suggests that there is slight improvement in thermal properties. SEM analysis revealed that CA/PSF 4 wt%, CA/PSF 6 wt% and CA/PSF 8 wt% blended membranes were less compatible and had less interfacial adhesion. The CO_2 gas seems to be more permeable through all membranes than H_2 owing to its ease of condensability and affinity with polar groups present in the CA/PSF blended membrane. Maximum selectivity of CO_2/H_2 was attained at CA/PSF 2 wt%, which did not further increase on addition of PSF. This reduction in selectivity is because of the agglomeration of PSF particles, which causes interfacial voids. In brief, it could be concluded that only 2 wt%PSF is completely miscible with CA and can be utilized for gas separation applications.

Table 4. Evaluation with reported blended membrane for CO_2/H_2 separation

Membrane	Fabrication method	Permeability of CO_2 (Barrer)	Permeability of H_2 (Barrer)	Selectivity CO_2/H_2	Permeation test condition	Reference
PVA-[EMIM][DCA] (9 wt%)	Solution casting	0.032	0.097	0.33	2 bar, 25 °C	[72]
PVA-[EMIM][DCA] (14 wt%)		0.097	0.335	0.29		
PVA-[EMIM][DCA] (24 wt%)		1.28	1.00	1.28		
PES/PVP (1 wt%)	Phase inversion	10	9	1.1	3 bar, 25 °C	[73]
PBI/PANI (5 wt%)	Solution casting	1.231	5.18	0.237	1.5 bar, 30 °C	[74]
PBI/PANI (10 wt%)		1.21	4.70	0.257		
PBI/PANI (15 wt%)		1.19	3.69	0.322		
cPIM-1/Torlon (10 wt%)	Solution casting	1,013	909.1	1.11	3.5 atm, 35 °C	[75]
cPIM-1/Torlon (90 wt%)		1.233	6.761	0.182		
CA/PSF (2 wt%)	Solution casting	80.51	43.90	1.83	2.5 bar, 25 °C	This work

ACKNOWLEDGEMENTS

We are pleased to acknowledge fastest flourishing, Membranes for applied research (MEMAR) lab, School of Chemical and Materials Engineering (SCME), National University of Science and Technology (NUST), Islamabad, Pakistan for providing lab facilities and HEC (Pakistan) grant No: 10032/Federal/NRPU/R&D/HEC/2017.

ABBREVIATIONS

PVA : polyvinyl alcohol
([EMIM][DCA]) : 1-ethyl-3-methylimidazolium dicyanamide
PBI : polybenzimidazole
PANI : polyaniline
cPIM-1 : carboxylate polymer of intrinsic micro porosity
S-PEEK : sulfonated poly ether- ether ketone
PEBAX 1657 : poly(ether-b-amide6)
GTA : glycerol triacetate
CA : cellulose acetate
PSF : polysulfone
MOF : metalorganic framework
CNTs : carbon nanotubes
ZIF : zeolitic imidazolate framework
CL : p-morpholinomethylcalixa arena
PES : polyether sulfone
PVP : polyvinylpyrrolidone

REFERENCES

1. L. Shao, B. T. Low, T.-S. Chung and A. R. Greenberg, *J. Membr. Sci.*, **327**, 18 (2009).
2. S. E. Hosseini and M. A. Wahid, *Renew. Sust. Energy Rev.*, **57**, 850 (2016).
3. X. Cao, H. Xu, S. Dong, J. Xu, Z. Qiao, S. Zhao, J. Wang and Z. Wang, *J. Membr. Sci.*, **601**, 117882 (2020).
4. S. E. Hosseini and M. A Wahid, *Renew. Sustain. Energy Rev.*, **57**, 850 (2016).
5. W.-H. Chen and C.-Y. Chen, *Appl. Energy*, **258**, 114078 (2020).
6. S.-I. Yang, D.-Y. Choi, S.-C. Jang, S.-H. Kim and D.-K. Choi, *Adsorption*, **14**, 583 (2008).
7. A. Hinchliffe and K. Porter, *Chem. Eng. Res. Des.*, **78**, 255 (2000).
8. G. O. Aksu, H. Daglar, C. Altintas and S. Keskin, *J. Phys. Chem.*, **124**, 22577 (2020).
9. S. D. Kenarsari, D. Yang, G. Jiang, S. Zhang, J. Wang, A. G. Russell, Q. Wei and M. Fan, *RSC Adv.*, **3**, 22739 (2013).
10. T. C. Merkel, M. Zhou and R. W. Baker, *J. Membr. Sci.*, **389**, 441 (2012).
11. J. D. Figueroa, T. Fout, S. Plasynski, H. McIlvried and R. D. Srivastava, *Int. J. Grnhouse Gas Control*, **2**, 9 (2008).
12. A. R. Nabais, A. P. Martins, V. D. Alves, J. G. Crespo, I. M. Marrucho, L. C. Tomé and L. A. Neves, *Sep. Purif. Technol.*, **222**, 168 (2019).
13. P. Li, Z. Wang, Z. Qiao, Y. Liu, X. Cao, W. Li, J. Wang and S. Wang, *J. Membr. Sci.*, **495**, 130 (2015).
14. Z. Kang, Y. Peng, Y. Qian, D. Yuan, M. A. Addicoat, T. Heine, Z. Hu, L. Tee, Z. Guo and D. Zhao, *Chem. Mater.*, **28**, 1277 (2016).
15. S. Japip, K. S. Liao and T. S. Chung, *Adv. Mater.*, **29**, 1603833 (2017).
16. H. Lin, Z. He, Z. Sun, J. Kniep, A. Ng, R. W. Baker and T. C. Merkel, *J. Membr. Sci.*, **493**, 794 (2015).
17. V. Vakharia, K. Ramasubramanian and W. W. Ho, *J. Membr. Sci.*, **488**, 56 (2015).
18. Y. Alcheikhhamdon and M. Hoorfar, *Chem. Eng. Process.*, **120**, 105 (2017).
19. A. Raza, S. Farrukh and A. Hussain, *J. Polym. Environ.*, **25**, 46 (2017).
20. J. Ø. Torstensen, R. M. Helberg, L. Deng, Ø. W. Gregersen and K. Syverud, *Int. J. Grnhouse Gas Control*, **81**, 93 (2019).
21. B. Lam, M. Wei, L. Zhu, S. Luo, R. Guo, A. Morisato, P. Alexandridis and H. Lin, *Polymer*, **89**, 1 (2016).
22. A. P. Isfahani, M. Sadeghi, A. H. S. Dehaghani and M. A. Aravand, *J. Ind. Eng. Chem.*, **44**, 67 (2016).
23. K. Kalantari, P. Moradihamedani, N. A. Ibrahim, A. H. B. Abdullah and A. B. M. Afifi, *Polym. Bull.*, **75**, 3723 (2018).
24. W. G. Lee and S. W. Kang, *Chem. Eng. J.*, **356**, 312 (2019).
25. H. Sanaeepur, A. E. Amooghin, S. Bandehali, A. Moghadassi, T. Matsuura and B. Van der Bruggen, *Prog. Polym. Sci.*, **91**, 80 (2019).
26. N. Tyan, G. Polotskaya, T. Meleshko, A. Yakimansky and Z. Pientka, *Russian J. Appl. Chem.*, **92**, 360 (2019).
27. K. Vanherck, G. Koeckelberghs and I. F. Vankelecom, *Prog. Polym. Sci.*, **38**, 874 (2013).
28. T. Puspasari, T. Chakrabarty, G. Genduso and K.-V. J. J. o. M. C. A. Peinemann, *J. Mater. Chem.*, **6**, 13685 (2018).
29. H. Abdul Mannan, H. Mukhtar, M. Shima Shaharun, M. Roslee Othman and T. Murugesan, *J. Appl. Polym. Sci.*, **133**, 42946 (2016).
30. M. Rezakazemi, A. E. Amooghin, M. M. Montazer-Rahmati, A. F. Ismail and T. Matsuura, *Prog. Polym. Sci.*, **39**, 817 (2014).
31. W. F. Yong and H. Zhang, *Prog. Mater. Sci.*, **116**, 100713 (2020).
32. H. Bai and W. W. Ho, *Ind. Eng. Chem. Res.*, **48**, 2344 (2009).
33. M. Klepić, K. Setničková, M. Lanč, M. Žák, P. Izák, M. Dendisová, A. Fuoco, J. C. Jansen and K. Friess, *J. Membr. Sci.*, **597**, 117623 (2020).
34. H. Rabiee, M. Soltanieh, S. A. Mousavi and A. Ghadimi, *J. Membr. Sci.*, **469**, 43 (2014).
35. S. R. Reijerkerk, M. H. Knoef, K. Nijmeijer and M. Wessling, *J. Membr. Sci.*, **352**, 126 (2010).
36. H. Sanaeepur, R. Ahmadi, M. Sinaei and A. Kargari, *J. Membr. Sci. Res.*, **5**, 25 (2019).
37. M. A. A. Hamid, Y. T. Chung, R. Rohani and M. U. Junaidi, *Sep. Purif. Technol.*, **209**, 598 (2019).
38. Z. Salahuddin, S. Farrukh and A. Hussain, *Int. J. Polym. Anal. Charact.*, **23**, 483 (2018).
39. J. Li, K. Nagai, T. Nakagawa and S. Wang, *J. Appl. Polym. Sci.*, **58**, 1455 (1995).
40. F. T. Minhas, S. Farrukh, A. Hussain and M. Mujahid, *J. Polym. Res.*, **22**, 63 (2015).
41. A. L. Khan, X. Li and I. F. Vankelecom, *J. Membr. Sci.*, **380**, 55 (2011).
42. M. Scandola and G. Ceccorulli, *Polymer*, **26**, 1953 (1985).
43. S. Farrukh, S. Javed, A. Hussain and M. Mujahid, *Asia-Pacific J. Chem. Eng.*, **9**, 543 (2014).
44. S. Kulprathipanja, *Ann. N. Y. Acad. Sci.*, **984**, 361 (2003).
45. S. Rafiq, Z. Man, A. Maulud, N. Muhammad and S. Maitra, *Sep. Purif. Technol.*, **90**, 162 (2012).

46. F. Dorosti, M. Omidkhah, M. Pedram and F. Moghadam, *Chem. Eng. J.*, **171**, 1469 (2011).
47. I. Salahshoori, D. Nasirian, N. Rashidi, M. K. Hossain, A. Hatami and M. Hassanzadeganroudsari, *Polym. Bull.*, **78**, 3227 (2020).
48. N. Benosmane, B. Guedioura, S. M. Hamdi, M. Hamdi and B. Boutemeur, *Mater. Sci. Eng. C.*, **30**, 860 (2010).
49. M. H. Rashid, S. Farrukh, S. Javed, A. Hussain, X. Fan, S. Ali and M. Ayoub, *Chem. Pap.*, **74**, 821 (2020).
50. P. D. Sutrisna, E. Savitri, M. A. Gunawan, I. H. F. Putri and S. G. de Rozari, *Polym.-Plast. Technol. Mater.*, **59**, 1300 (2020).
51. T. Kallel, V. Massardier-Nageotte, M. Jaziri, J. F. Gérard and B. Elleuch, *J. Appl. Polym. Sci.*, **90**, 2475 (2003).
52. A. Codou, A. Anstey, M. Misra and A. K. Mohanty, *RSC Adv.*, **8**, 15709 (2018).
53. J. D. Moon, A. T. Bridge, C. D'Ambra, B. D. Freeman and D. R. Paul, *J. Membr. Sci.*, **582**, 182 (2019).
54. Y. Miyashita, T. Suzuki and Y. Nishio, *Cellulose*, **9**, 215 (2002).
55. M. Mubashir, Y. F. Yeong, K. K. Lau, T. L. Chew and J. Norwahyu, *Sep. Purif. Technol.*, **199**, 140 (2018).
56. E. Saljoughi, M. Amirilargani and T. Mohammadi, *Desalination*, **262**, 72 (2010).
57. P. A. Vinodhini, K. Sangeetha, G. Thandapani, P. Sudha, V. Jayachandran and A. Sukumaran, *Int. J. Biol. Macromol.*, **104**, 1721 (2017).
58. H. Wu, X. Fang, X. Zhang, Z. Jiang, B. Li and X. Ma, *Sep. Purif. Technol.*, **64**, 183 (2008).
59. S. Thanakkasaranee, D. Kim and J. Seo, *Polymers*, **10**, 225 (2018).
60. P. A. Vinodhini, K. Sangeetha, G. Thandapani, P. Sudha, V. Jayachandran and A. Sukumaran, *Int. J. Biol. Macromol.*, **104**, 1721 (2017).
61. M. Gaur, P. K. Singh and R. S. Chauhan, *J. Therm. Anal. Calorim.*, **111**, 743 (2013).
62. P. Sajjan, V. Nayak, M. Padaki, V. Y. Zadorozhnyy, S. N. Klyamkin and P. J. E. Konik, *Fuels*, **34**, 11699 (2020).
63. I. Shakeel, A. Hussain and S. Farrukh, *J. Polym. Environ.*, **27**, 1449 (2019).
64 M. Gaur, P. K. Singh and R. Chauhan, *J. Therm. Anal. Calorim.*, **111**, 743 (2013).
65. S. Vetrivel, M. S. A. Saraswathi, D. Rana and A. Nagendran, *Int. J. Biol. Macromol.*, **107**, 1607 (2018).
66. C. Makhloufi, D. Roizard and E. Favre, *J. Membr. Sci.*, **441**, 63 (2013).
67. Y. P. Chen, S. Bashir and J. L Liu, *Nanostructured materials for next generation energy storage and conversion: hydrogen production, storage, and utilization*, Springer, Heidelberg (2017).
68. M. A. Abd Hamid, Y. T. Chung, R. Rohani and M. U. Mohd Junaidi, *Sep. Purif. Technol.*, **209**, 598 (2019).
69. P. N. Khanh, N. T. Trung and H. Srour, *Carbon dioxide chemistry, capture and oil recovery*, intechopen, London (2018).
70. M. Raouf, R. Abedini, M. Omidkhah and E. Nezhadmoghadam, *Process Saf. Environ. Prot.*, **133**, 394 (2020).
71. A. Mondal and B. Mandal, *J. Membr. Sci.*, **446**, 383 (2013).
72. M. Klepić, K. Setničková, M. Lanč, M. Žák, P. Izák, M. Dendisová, A. Fuoco, J. C. Jansen and K. Friess, *J. Membr. Sci.*, **597**, 117623 (2020).
73. S. Yousef, J. Šereika, A. Tonkonogovas, T. Hashem and A. Mohamed, *J. Environ. Technol. Innovation*, **21**, 101339 (2021).
74. V. Giel, J. Kredatusová, M. Trchová, J. Brus, J. Žitka and J. Peter, *Eur. Polym. J.*, **77**, 98 (2016).
75. W. F. Yong, F. Y. Li, T. S. Chung and Y. W. Tong, *J. Membr. Sci.*, **462**, 119 (2014).